Design of a Teleoperated Needle Steering System for MRI-guided Prostate Interventions

Reza Seifabadi, Iulian Iordachita, and Gabor Fichtinger

Abstract- Accurate needle placement plays a key role in success of prostate biopsy and brachytherapy. During percutaneous interventions, the prostate gland rotates and deforms which may cause significant target displacement. In these cases straight needle trajectory is not sufficient for precise targeting. Although needle spinning and fast insertion may be helpful, they do not entirely resolve the issue. We propose robot-assisted bevel-tip needle steering under MRI guidance as a potential solution to compensate for the target displacement. MRI is chosen for its superior soft tissue contrast in prostate imaging. Due to the confined workspace of the MRI scanner and the requirement for the clinician to be present inside the MRI room during the procedure, we designed a MRI-compatible 2-DOF haptic device to command the needle steering slave robot which operates inside the scanner. The needle steering slave robot was designed to be integrated with a previously developed pneumatically actuated transperineal robot for MRI-guided prostate needle placement. We describe design challenges and present the conceptual design of the master and slave robots and the associated controller.

I. Introduction

Prostate cancer is the most common cancer in men in the United States, as well as in the western hemisphere. According to the statistics, each year approximately 1.5 million prostate biopsy procedures are performed in the United States [1]. Following positive transrectal ultrasound (TRUS) guided needle biopsy, many patients choose brachytherapy as a minimally invasive definitive treatment. Brachytherapy entails the implantation of 60-120 radioactive pellets (seeds) into the prostate. Transrectal ultrasound is the gold standard guidance method for both prostate biopsy and brachytherapy. In either biopsy or brachytherapy, needles are manually inserted into the prostate along straight trajectory under real-time TRUS guidance. TRUS is inexpensive and readily accessible, but it is inadequate for visualizing cancer [2] and the implanted seeds. MRI provides a promising alternative to ultrasound due to its excellent visualization of the prostate gland and its substructures, focal lesions within the gland, and surrounding tissues.

Major shortcomings of conventional manual needle placement include lack of the ability to provide angulation,

which is critical to avoid pubic arch interference, as well as limited accuracy and repeatability.

Several MRI-compatible robots have been reported for prostate interventions. They are categorized as transrectal, transperineal, and transgluteal, according to the way they access the prostate. MRI-guided transperineal prostate interventions were studied in patient experiments inside open MRI scanner by Chinzei [3]. In [4], Di Maio designed a system to assist transperineal intra-prostatic needle placement. In [5], Tadakuma developed a MRI-compatible robot for transperineal needle placement using dielectric elastomer actuators (DEAs). In [6], Stoianovici developed a pneumatically actuated device for transperineal brachytherapy seed placement. In [7], Fischer developed a pneumatic 2-DOF robot for transperineal prostate needle placement.

Generally, robot provides needle orientation toward a predefined target based on intraoperative images, and the needle is usually inserted manually. However, there is always notable targeting error due to prostate rotation and deformation, as well as to needle deflection. To reduce the insertion force and consequently reduce the abovementioned error, different needle insertion strategies have been proposed. In [8], Lagerburg reports a tapping method to decrease the insertion force. In [9], Muntener reports a fast needle insertion. In [10], Badaan reports needle rotation as a useful tool to reduce the friction force and therefore, to reduce the displacement error. However, these methods do not solve the problem entirely. Moreover, they reduce the risk to the patient safety in the case of fast insertion or may cause tissue damage in the case of needle spinning.

Needle deflection is an important source of targeting error [11]. However, one may take advantage of it in a positive way and employ it to compensate for the targeting error. In fact, if a bevel-tip needle is rotated during insertion for 180 degrees, the lateral force applied to the needle tip will maneuver the needle in opposite direction. This idea is called bevel-tip needle steering and was initially proposed to generate curved trajectories [12] for avoiding obstacles inside soft tissues. In this paper we use a similar idea for accuracy improvement.

Needle steering can be either computer-controlled (automated) or human-controlled. Each of these approaches has its own pros and cons. For example, the computer-controlled approach may be faster and provide less trauma to the patient as it requires fewer insertions. However, a decent

R. Seifabadi and G. Fichtinger are with Laboratory for Percutaneous surgery (Perk Lab), Queen's University, Kingston, ON, Canada.
I. Iordachita is with Laboratory for Computational Sensing and Robotics (LCSR), The Johns Hopkins University, Baltimore, MD, USA.
Corresponding author: reza.seifabadi@queensu.ca

tissue model is necessary as well as a sophisticated controller algorithm or alternatively, a nearly real-time image feedback which is not available in most of today's MRI scanners. On the contrary, the human-operated needle steering requires neither a mechanical model of the tissue nor sophisticated control architecture. It also does not require a very high quality MRI image and even an imaging sample frequency of 2Hz might be enough [13] since a human is still maneuvering the needle. The biggest advantage is having a human in the loop, thus being less risky to the patient and more trusted by clinicians. Due to the advantage of clinician presence in the loop and the relative simplicity of the system design, we chose a human-operated approach in this study.

The scanner bore confined workspace (typically a 60 cm in diameter, 2 meter long) makes most manual operations infeasible. Therefore, the suggested human-operated needle steering device should be commended remotely. We propose a teleoperated needle steering scenario in which a robot with similar kinematics (called master) will control the needle steering module (called slave).
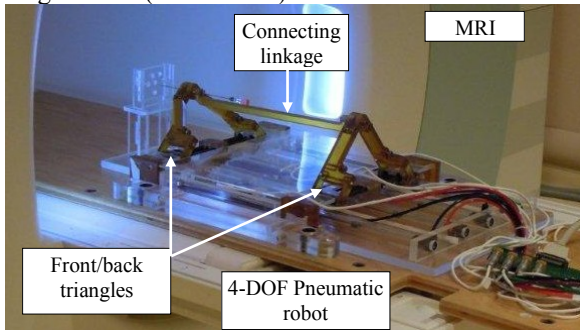

Fig. 1. The slave robot was designed for a previously developed 4-DOF pneumatic robot for MRI-guided transperineal prostate biopsy.

During interventions, clinicians prefer to stay beside the patient so they can make an appropriate decision if unwanted events occur. This requires that not only the slave robot that operates inside MRI scanner, but also the master robot should be MRI-compatible. Commercially available haptic devices, therefore, cannot be employed. One of our challenges would be to design a haptic device which is MRI-compatible and also appropriate for needle steering task.

In this paper, we propose a teleoperated needle steering system under MRI guidance to compensate for targeting errors caused during percutaneous prostate interventions. This realizes the capability of remote needle insertion while the patient is inside the bore, as suggested in [14]. This system is designed to be integrated with a previously developed pneumatic robot for MRI-guided prostate interventions [15] with negligible design changes (Fig. 1). The focus of this paper is placed on the system design. Conceptual designs for the master and slave are provided.

II. Robotic system architecture

Figure 2 shows the information flow of the robotic system for MRI-guided prostate intervention. In the MRI room, the slave robot is placed on top of the MRI table,

between the patient's legs. The controller is placed next to the scanner (red items are added in this study and will be discussed later. The planning and navigation workstation (based on 3D Slicer), scanner console, and power supply are located in the control room. The air pressure required for the robot actuation is provided through the air pressure line of the hospital. A local network is set up to enable data transfer among the scanner, robot controller, and navigation and planning software.
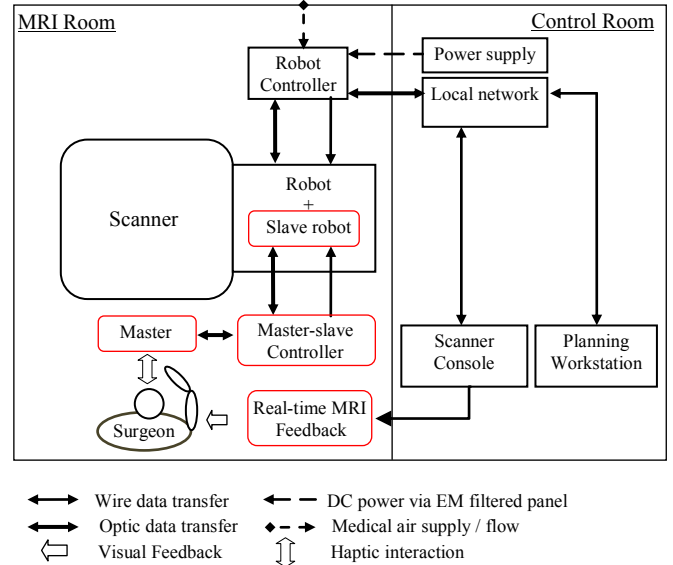

Fig. 2. Diagram of the robotic system components and information flow. Red squares show new added components to the previous setup.

The clinical workflow of the robotic assistant system before implementation of master-slave needle steering is as follows: (1) a diagnostic image is taken from the patient; (2) this image is sent to the planning and navigation workstation; (3) a target is specified by the specialist within the prostate capsule; (4) target coordinates are sent to robot controller; (5) the robot orients the needle toward specified target; and (6) the patient is pulled out of the scanner and the needle is inserted manually.

Due to prostate motion and deformation and needle deflection, the needle tip will not necessarily reach the desired position. In order to compensate for this error, we propose a teleoperated needle steering approach under the currently available real-time MRI guidance technology (Fig. 2). In fact, if surgeons see any divergence from the straight path (5 mm for the case of biopsy) during the needle advancement, they can slightly retract the needle, rotate the bevel-tip needle for 180 degrees so the needle bends toward the opposite direction and reduce the error. The assumption is that the pneumatic robot is highly accurate [11] and the real-time MRI image has adequate spatial resolution. The surgeon stays next to the scanner/patient and interacts with a master device which has similar kinematics to the needle steering slave robot. A MRI-compatible monitor provides in-the room real-time MRI image for clinician. A controller is designed and implemented to communicate between the master and the slave robots and is placed next to the scanner.

This controller is different from the previously developed controller which provides 4-DOF for the pneumatically actuated base robot. The newly added components are marked in red in Fig 2. In the following sections, we will describe these components in detail.

III. Slave robot

The slave robot (i.e. needle steering module) main function is to generate simultaneous linear and rotary motions for the bevel-tip needle such that needle steering becomes possible. This module replaces the linkage connecting the base robot front and back triangles (Fig. 1). Figure 3 shows the CAD design of the needle steering module. The linear DOF is produced by a belt drive consisting of the rotary piezo motor M1, pulley P2 and P3 and the timing belt, T (Fig. 3). A piezo motor is used for its high precision, ease of control, and most importantly, MRI-compatibility [16]. Pneumatic and hydraulic actuators are not used due to high nonlinearity and difficulty of control for the former and risk of leakage for the latter. The timing belt T is attached to guide H and moves it as the motor rotates. The guide slides along two aluminum anodized shafts through two linear bearings. The rotary motion is provided by a second motor which travels with the guide H and transmits the rotation via a small timing belt (up-down). There are two reasons for choosing a belt drive for linear motion. First, it is more energy efficient than other conventional methods such as lead-screw. This is important for bilateral teleoperation systems since friction could be misinterpreted as insertion force. Also, due to the restriction of MRI-compatibility, we are limited to using certain piezo motors (PiezoLEG 80 N.mm, 20 RPM, Uppsala, Sweden) with small output torque (80 N.mm) which again poses minimizing the amount of friction. Second, belt drive has a minimum backlash. Linear motors were avoided for compactness.
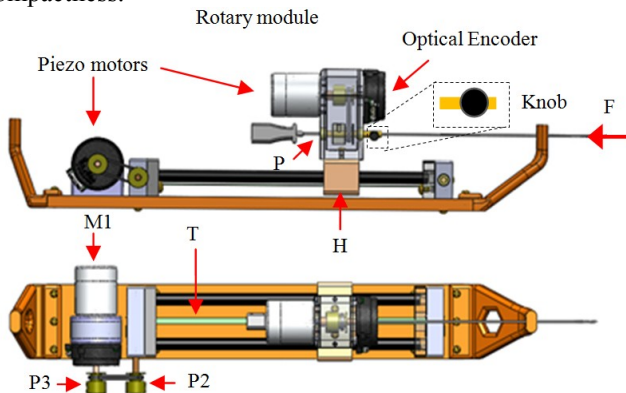

Fig. 3. CAD design of the slave robot: front and top views

Other slave robot design criteria are: (1) slave robot must be MRI-compatible. Therefore, all parts were made of plastic and non-magnetic materials. Piezo motors and optical encoders (US Digital, Vancouver, WA) are used for the same purpose; (2) the module should provide a travel of 140 mm such that deep targets could be reached inside the prostate capsule; (3) needle should be able to rotate 360 degrees both sides to enable needle steering at any direction; and (4) the module should be able to supply constant force of 3.2 N (enough for inserting a 20G needle into the prostate - see next section for the logic) at the speed of 5 mm/sec. In order to reach such speed, the angular velocity of pulley P2 should be 15 rpm. Therefore, we consider a gear ratio of 1.5:1 between pulleys P3:P2 since the motor alone cannot provide this speed according to the Piezo motor torque-speed diagram (http:// www. piezomotor.se). At this speed (10 rpm), the maximum output torque at motor's shaft is 30 N.mm which corresponds to 20 N.mm at pulley P2 and can generate an insertion force of 6.2 N (more than the desired 3.2 N).

In the case of power failure, the needle holds its own position due to the inherent friction of the piezo motor, which acts as a measure for the patient safety. The needle can be easily loaded (and retracted) from the point P (Fig. 3) and fixed axially by a thumb knob. The needle holder has an inner tube which is removable and sterilizable. Fig. 4 shows the needle steering module integrated to the 4-DOF pneumatic robot.
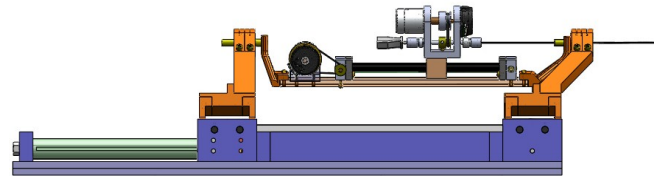

Fig. 4. The needle steering module is integrated to the 4-DOF pneumatic robot

IV. Master robot

The master robot is used to perform needle steering remotely from outside the scanner. Therefore, we no longer need to remove the patient for needle placement. As a result, the operation duration is shortened and the inaccuracies caused by patient movement can be minimized.

For the purpose of MRI-compatibility, conventional haptic devices cannot be employed. Therefore, we designed a MRI-compatible haptic device appropriate for needle steering. Similar to the needle steering device, it has 2-DOF: translation for needle advancement and needle rotation. Figure 5 shows the CAD design of the proposed mechanism. The clinician grabs a small diameter cylinder (stylus) mimicking the needle and manipulates it as real needle steering is done, i.e. inserting the needle and rotating it if necessary.

In the context of haptic design, it is important to minimize inertia of the moving parts and friction force since they distort kinesthetic sense. This suggests that the actuators should be stationary and that light weight transmission mechanisms such as cable-driven mechanisms are preferred. High friction joints should also be avoided. In our design, we have tried to take these criteria into consideration.

To generate the translational motion, i.e. needle insertion, a mechanism that converts rotary motion (of a fixed actuator) into linear motion with minimum friction is desirable. Different mechanisms were considered [17, 18].
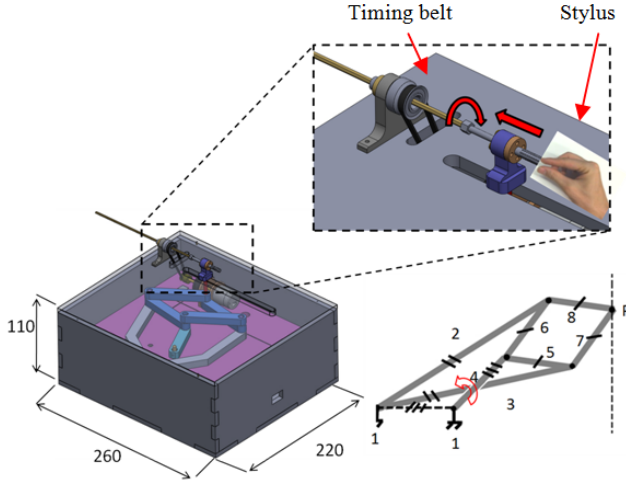
Fig. 5. CAD design of the master robot: Peaucellier-Lipkin mechanism is employed to convert rotary motion of motor to perfect linear motion.

One possibility is using four bar linkages that generate a straight trajectory such as Chebyshev, Hoeken, and Watt linkages. However, they are bulky, the trajectory is not perfectly linear, and the straight trajectory is only part of the whole trajectory. Instead, we propose using the Peaucellier-Lipkin mechanism shown in Fig. 6. Some advantages of this mechanism are as follows: (1) there is no sliding joint in this mechanism meaning that friction is minimal; (2) its effector generates a perfect line throughout the track; (3) it is compact; and (4) counter balancing is not necessary since the mechanism can be configured horizontally. The actuator is placed stationary at joint B. Links AE and AD are equal in length and so are CE, EP, PD, and DC. As BC rotates, P travels an accurate straight line meaning that P= (d, y) where d is a constant.

Kinematic analysis: A and C lie on a circle which is centered on B. It can be easily proved that A, C, and P are collinear. Therefore, $\beta = 2\alpha$. Thus,

$$y = d \times \tan(\alpha) = d \times \tan(\beta/2) \leftrightarrow \qquad (1)$$

$$\beta = 2\,Atang\left(\frac{y}{d}\right)$$

It can be shown that:

$$d = \frac{l_1^2 - l_3^2}{2l_2} \qquad (2)$$

where l_1 = AD, l_2 = BC, and l_3 = CD.

Equation (1) expresses the relationship between β, as input and translation of point P as output and vice versa. Equation (2) is used for designing the sizes of linkages as well as power analysis.

Dynamic analysis: Having the force that operator applies to the master robot stylus during insertion, the required torque of the motor is sought. For the specific application of this haptic device, the maximum needle insertion speed is 7 mm/sec.
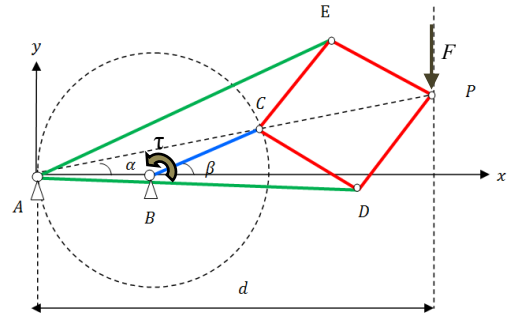

Fig. 6. Peaucellier-Lipkin mechanism geometry

The linkages are made of plastics (acrylic and rapid prototype stereolithography resins) making them light. Therefore, the quasi static assumption would be a fair assumption for dynamic analysis. From energy conservation law and assuming negligible friction loss in joints, one has:

$$Power_{in} = Power_{out} \rightarrow \tau.\dot{\beta} = F.\dot{y} \rightarrow$$

$$\tau = F.\frac{\dot{y}}{\dot{\beta}} = F\frac{dy}{d\beta} \xrightarrow{from\,(1)}$$

$$\tau = F\frac{d}{2}\left(1 + tan^2\left(\frac{\beta}{2}\right)\right) = F\frac{d}{2}\left(1 + \left(\frac{y}{d}\right)^2\right) \qquad (3)$$

This means the torque supplied by the motor must increase quadratically with y. Figure 7 shows this relationship.
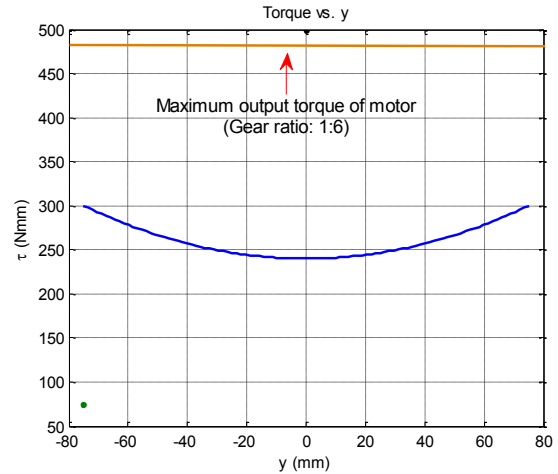

Fig. 7. Torque required to be supplied by motor as a function of needle displacement

Link sizing and power analysis: The first constraint in the link size design is travel in y direction which is 150 mm (10 mm longer than the slave robot's travel). The second constraint is the linearity of the input-output relationship, which, although it does not cause inaccuracy at the end-effector, is desired [10]. We divided the 150 mm travel symmetrically (±75 mm) around the origin in order to maximize the input-output linearity (Fig. 8). The third constraint is power consumption; it is desirable to use a single 80 N.mm piezoelectric motor for the translation DOF for the sake of compactness, simplicity of design and control. This constraint means d should be as small as

possible according to equation (3). Power minimization is of higher importance than input-output linearity since the latter could be compensated for. Therefore, linearity can be somehow compromised for power minimization.
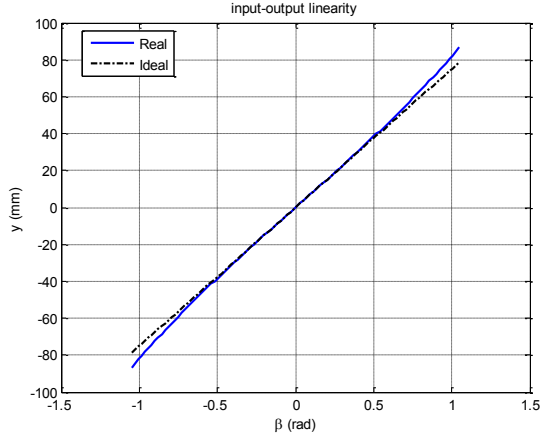

Fig. 8. The input-output relationship remains satisfactorily linear if β is bounded to $[-\pi/3, \pi/3]$.

In the literature, the average force for transperineal brachytherapy is measured to be 6 and 5 N for 17G and 18 G needles, respectively [19]. For needle steering application, the thickest needle which is flexible enough is 20G in size. Since we do not have similar data for inserting 20G needle into the prostate, we employed an extrapolation as shown in Table 1.

Table 1. Average insertion force of different brachytherapy needles

Needle	Avg insertion force (N)	Diameter (mm)
17G	6	1.47
18G	5	1.27
20G	3.2	0.91

Hence, the expected average force would be 3.2 N. However, the maximum force applied to the needle during needle insertion might be higher and for this purpose, the supplied torque by the motor should be higher than this average (Fig. 7).

Assuming that $y = 75$ mm occurs at $\beta = \pi/6$, from equation (1), we have $d = 280\ mm$. This means the required maximum torque is 450 N.mm which is almost 6 times as large as the nominal output of the piezoelectric motor. In other words, a minimum gear ratio of 1:6 is required to achieve this large torque. To avoid this relative high gear ratio, we slightly compromise the linearity. Let us design d to be 150 mm. This means the maximum β is 0.93 which is still below 1 and the linearity is satisfactory according to Figure 8. Thus, the maximum required torque would be 300 N.mm which can be satisfied with a gear ratio of 1:4. Also, according to (2) and considering $l_2 = 50$ mm, $l_1 = 140$ mm, and $l_3 = 70$ mm, $d = 147$ mm which closely correlates with the desired value of 150 mm.

Some other design considerations are as follow: (1) both motors and encoders are fixed to the base for minimal inertia; (2) for the rotary DOF, a timing belt is used to transmit the power from the piezo motor to the stylus (Fig. 5,

9); (3) all materials are non-ferromagnetic; and (4) the friction is minimized as the result of choosing the Peaucellier-Lipkin mechanism.
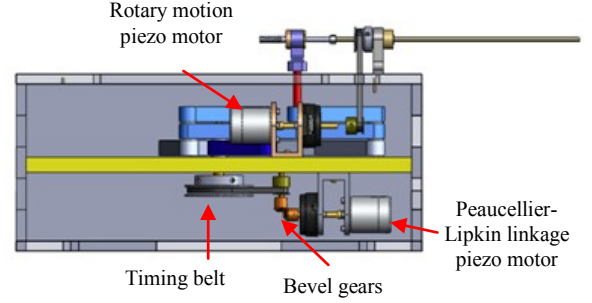

Fig. 9. Internal view of the master robot

V. Controller

The controller unit consists of four PDA 3.1 piezo motor drivers (PDA 3.1, PiezoMotor, Upsala, Sweden), a DMC-2143 Ethernet motion controller (Galil Motion Control, Rocklin, California), and a laptop on which GalilTools (the software to command the controller and to monitor encoders' signals) runs. A 24 V DC power supply is used to run the controller and drivers. There are two controllers, one for the master and one for the slave. The role of these controllers is to ensure position tracking between the master and slave position signals. The teleoperated system block diagram (master, slave and their controllers- this excludes the controller of the pneumatic robot [7]) is shown in Figure 10.
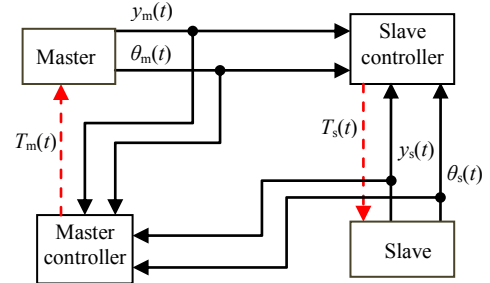

Fig. 10. Teleoperated system block diagram

$y_m(t)$ and $\theta_m(t)$ and $y_s(t)$ and $\theta_s(t)$ are translational and rotational motions of the master and slave, respectively. $T_\Delta(t)$ is the control signal for the master and slave robot and is defined as follows:

$$T_\Delta = [T_y^\Delta, T_\theta^\Delta]^T \quad (4)$$

$\Delta = \{m,\ s\}$ where m and s stand for master and slave, respectively.

$$T_y^\Delta(t) = KP_\Delta^{Tr}.\delta.\big(y_m(t) - y_s(t)\big)$$
$$+ KI_\Delta^{Tr} \int_0^t \delta.[y_m(t) - y_s(t)]dt$$
$$T_\theta^\Delta(t) = KP_\Delta^{Ro}.\delta.\big(\theta_m(t) - \theta_s(t)\big) \quad (5)$$
$$+ KI_\Delta^{Ro} \int_0^t \delta.[\theta_m(t) - \theta_s(t)]dt$$

T_y^Δ and T_θ^Δ are the control laws for the translational and rotational actuators. KP_Δ^{Tr} and KI_Δ^{Tr} are proportional and integral gains for the translational motors while KP_m^{Ro} and KI_m^{Ro} are proportional and integral gains for the rotational motors. $\delta = 1$, if $\Delta = m$ and it is equal to -1, if $\Delta = s$.

VI.   Conclusions and future works

In this study, teleoperated needle steering under real-time MRI guidance was proposed as a potential solution to compensate for targeting error caused by different sources including prostate deformation, prostate motion and needle deflection. From this end, a 2-DOF MRI-compatible master-slave system was designed. Design challenges were discussed for the master and slave robots. This system was designed such that it could be integrated with a currently developed pneumatic robot for MRI-guided prostate intervention with negligible design changes. A prototype of the slave robot was built and the simple controller was proposed for the teleoperatory system.

In the future, after the master and slave robots are built, phantom experiments will be conducted to ensure needle steering feasibility as well as accuracy.

ACKNOWLEGEMENTS

REFERENCES

[1]   R. Siegel, E. Ward, O. Brawley, and A. Jemal. Cancer Statistics, 2011. The impact of eliminating socioeconomic and racial disparities on premature cancer deaths, Figure 1, DOI: 10.3322/caac.20121.

[2]   M.K. Terris, E.M. Wallen, and T.A. Stamey. Comparison of mid-lobe versus lateral systematic sextant biopsies in detection of prostate cancer. *Urol. Int.*, vol. 59, pp. 239–242, 1997

[3]   K. Chinzei, N. Hata, F. A. Jolesz, and R. Kikinis. MR compatible surgical assist robot: System integration and preliminary feasibility study. In *Medical Image Computing and Computer-Assisted Intervention* (*MICCAI*), vol. 1935, pp. 921–930, 2000.

[4]   S. P. DiMaio, S. Pieper, K. Chinzei, N. Hata, S. J. Haker, D. F. Kacher, G. Fichtinger, C. M. Tempany, and R. Kikinis. Robot-assisted needle placement in open MRI: system architecture, integration and validation. *Computer Aided Surgery*, vol. 12(1), pp. 15–24, 2007.

[5]   K. Tadakuma, L. M. DeVita, J. S. Plante, Y. Shaoze, and S. Dubowsky. The experimental study of a precision parallel manipulator with binary actuation: With application to MRI cancer treatment. In Proc. *IEEE International conference on Robotics and Automation (ICRA)*, pp. 2503 - 2508, Pasadena, USA, 2008.

[6]   D. Stoianovici, D. Song, D. Petrisor, D. Ursu, D. Mazilu, M. Muntener, M. Mutener, M. Schar, and A. Patriciu. MRI stealth robot for prostate interventions. *Minimally Invasive Therapy and Allied Technologies*, vol. 16(4), pp. 241–248, 2007.

[7]   G. S. Fischer, I. Iordachita, C. Csoma, J. Tokuda, S. P. DiMaio, C. M. Tempany, N. Hata, and G. Fichtinger. MRI-compatible pneumatic robot for transperineal prostate needle placement. *IEEE/ASME Transactions on Mechatronics*, vol. 13(3), pp. 295–305, 2008.

[8]   V. Lagerburg, M.A. Moerland, M.K. Konings, R.E. Van de Vosse, J.J.W. Lagendijk, and J.J. Battermann. Development of a tapping device: a new needle insertion method for prostate brachytherapy, *Phys. Med. Biol.* vol. 51 (4), pp. 891–902, 2006

[9]   M. Muntener, A. Patriciu, D. Petrisor, D. Mazilu, H. Bagga, L.R. Kavoussi, K. Cleary, and D. Stoianovici, "MRI-compatible robotic system for fully automated brachytherapy seed placement," *Urology*, vol. 54 (8), pp. 1499 –1506, 2006

[10]   S. Badaan, D. Petrisor, C. Kim, P. Mozer, D. Mazilu, G. Gruionu, A. Patriciu, K. Cleary, D. Stoianovici. Does needle rotation improve lesion targeting? *International Journal of Robotics and Computer Assisted Surgery*, vol. 7(2), pp. 138–147, 2011

[11]   R. Seifabadi, N. B. Cho, S. E. Song, J. Tokuda, N. Hata, C. M. Tempany, G. Fichtinger, and I. Iordachita, "Acuracy Study of a MRI-guided Robotic System for Prostate Biopsy", The *International Journal of Medical Robotics and Computer Assisted Surgery* (IJMRCAS), in press,

[12]   S.P. DiMaio, S.E. Salcudean. Needle steering and model-based trajectory planning, In *Medical Image Computing and Computer-Assisted Intervention* (*MICCAI*), vol. 2878, pp. 33-40, 2003

[13]   H. Su, M. Zervas, G. Cole, C. Furlong, and G. Fischer. Real-time MRI-guided needle placement robot with integrated fiber optic force sensing. In Proc. *IEEE International Conference on Robotics and Automation (ICRA)*, pp. 1583–1588, Beijing, China, 2011.

[14]   R. Seifabadi, S. E. Song, A. Krieger, J. Tokuda, G. Fichtinger, and I. Iordachita, "Robotic System for MRI-guided Prostate Biopsy: Feasibility Study of Tele-operated Needle Insertion and ex-vivo Phantom Study*", International Journal of Computer Aided Radiology and Surgery* (IJCARS), vol 7 (2), pp 181-190, Springer, 2012

[15]   S.E. Song, N.B. Cho, G. Ficsher, N. Hata, C.M. Tempany, G. Fichtinger, and I. Iordachita. Development of a pneumatic robot for MRI-guided transperineal prostate biopsy and brachytherapy: New approaches. In Proceeding of *IEEE International Conference Robotic and Automation (ICRA)*, pp. 2580-2585 Anchorage, USA, 2010.

[16]   H. Su, D. Cardona, W. Shang, G. Cole, C. Rucker, R. Webster III and G. Fischer, "A MRI-Guided Concentric Tube Continuum Robot with Piezoelectric Actuation: A Feasibility Study", *IEEE ICRA 2012 International Conference on Robotics and Automation*, Saint Paul, Minnesota, USA, 2012

[17]   L. Barbé, B. Bayle, O. Piccin, J. Gangloff, and M. de Mathelin. Design and evaluation of a linear haptic device. Proceedings *IEEE International Conference on Robotics and Automation* (*ICRA*), Italy, pp. 485 – 490, 2007

[18]   D. Stoianovici, K. Cleary, A. Patriciu, D. Mazilu et al. AcuBot: A Robot for Radiological Interventions. *IEEE Transactions on Robotics and Automation*. vol. 19, pp. 926–30, 2003

[19]   T.K. Podder, D.P. Clark, J. Sherman, E.M. Messing, D. Fuller, D.J. Rubens, *et al*. In vivo Motion and Force Measurement of Surgical Needle Intervention during Prostate Brachytherapy. *Journal of Medical Physics*, vol. 33(8), pp. 2915-2922, 2006